www.ietdl.org

Published in IET Communications
Received on 13th September 2013
Revised on 3rd February 2014
Accepted on 20th February 2014
doi: 10.1049/iet-com.2013.0815

ISSN 1751-8628

Ultra-wideband-based multilateration technique for indoor localisation

Oladimeji Onalaja, Mounir Adjrad, Mohammad Ghavami

Faculty of Engineering, Science and the Built Environment, London South Bank University, London SE1 0AA, UK
E-mail: onalajao@lsbu.ac.uk

Abstract: In this study, the authors present a novel geometrically driven multilateration technique that is based on ultra-wideband (UWB) technology. The authors refer to their proposed solution as time reflection of arrival (TROA). They demonstrate in this study how the position estimation error is improved upon by carefully considering the inherent properties of the UWB technology and the reflection properties of transmitted UWB signals. By a direct comparison between TROA and two widely used multilateration techniques, the authors show that indoor position estimation can be done much more effectively using their proposed solution. They also derive a new Cramér–Rao lower bound for TROA multilateration and use it to show its level of efficiency.

1 Introduction

Position estimation problems have seen an exponentially increased interest in recent years [1–7]. Position estimation techniques are generally based on two underlying principles namely 'geometric multilateration' and 'statistical multilateration' [8, 9]. Geometric multilateration techniques estimate position by using the geometrical link resulting from signal propagation between a node of interest (NOI), neighbouring reference nodes and base stations. Its variants include time of arrival (TOA), time difference of arrival (TDOA), time sum of arrival (TSOA), the received signal strength and the angle of arrival [1–4, 8, 9]. Statistical multilateration techniques such as Aso *et al.* [5], Man-Kin Chu *et al.* [6] and Roos *et al.* [7] estimate position by means of statistical modelling of error bounds and other stochastic models. TSOA-based multilateration techniques have reached limitations with regards to the current increased demand for enhanced accuracy of indoor position estimation techniques. As the authors of [8–10] explain, the general consensus seems to be that they do not provide any additional performance advantage(s) over other widely used hyperbolic-based multilateration techniques. In this work, we prove this theory to be right by means of a direct comparison with the TOA multilateration technique as well as our proposed technique. However, and much more significantly, in this work, we build up on the fundamental working principles of the TSOA-based multilateration technique and use it to derive a novel technique which we coin as time reflection of arrival (TROA). We derive a theoretical lower bound on the covariance of the TROA estimator based on the Cramér–Rao lower bound (CRLB), and show that our proposed approach achieves relatively good operational performances when the mean squared error (MSE) implications are considered. The rest of this paper is organised as follows: Section 2 details an introduction into the concept of TSOA multilateration; Section 3 illustrates our proposed system's basic functionality right from its initial conception, and also bridges any inadvertent knowledge gap between its conceptualisation, practical ramifications and theoretical accuracy. Section 6 discusses the ultra-wideband (UWB) channel modelled for the proposed TROA multilateration scheme; Section 5 validates our system by means of simulation results and CRLB analysis; and Section 4 summarises and concludes this work.

2 Background

TSOA multilateration involves the propagation of signals from an NOI to known and fixed reference nodes ($RN_{i=1,2,3,\ldots,\infty}$) or anchors [8]. The reference nodes are typically receivers and conventionally, the NOI is required to be either active (i.e. a mobile station) or semi-passive (i.e. a semi-passive radio frequency identification tag), or alternatively have an inherently active or semi-passive component that facilitates its signal propagation to the various reference nodes required for multilateration [8, 9]. As depicted in Fig. 1, following the signal propagation from the NOI, two reference nodes are usually paired together to generate a range sum estimate. This range sum estimate is then used to define a conic section whose semi-major axis is always greater than its semi-minor axis (i.e. an ellipse) [11]. With reference to Fig. 1, and considering the pairing between RN_1 and RN_2, the range sum is defined as the algebraic sum of D_{NOI-RN_1} (distance between NOI and RN_1) and D_{NOI-RN_2} (distance between

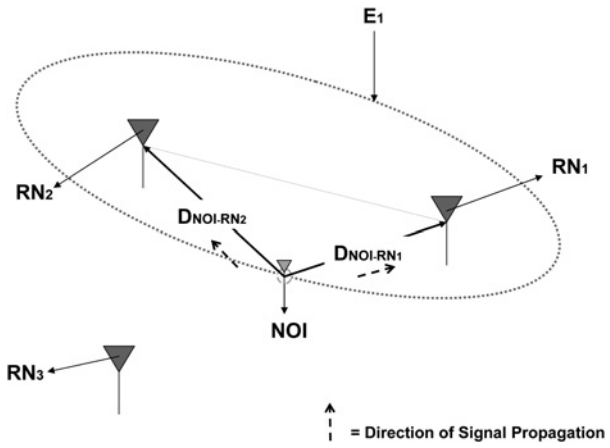

Fig. 1 *Generation of a single ellipse using two RNs*

NOI and RN_2). Assuming a line-of-sight (LOS) separation between the NOI and both reference nodes, D_{NOI-RN_1} and D_{NOI-RN_2} are determined by multiplying the arrival time of the signal propagated from the NOI to RN_1 and RN_2, respectively, by c (i.e. speed of light). The general equation for the defined ellipse (E_i) based on the range sum is given by (1) where (h_1, k_1) is its centre coordinate, a_1 is its semi-major axis and b_1 is its semi-minor axis [11]

$$\frac{(x_i - h_i)^2}{a_i^2} + \frac{(y_i - k_i)^2}{b_i^2} = 1 \tag{1}$$

Denoting E_1 of centre coordinate (h_1, k_1), semi-major axis a_1 and semi-minor axis b_1 as the ellipse defined by the pairing between RN_1 and RN_2, when a third reference node (RN_3) is introduced and paired with RN_2 just as Fig. 2 depicts, another ellipse (E_2) with centre coordinate (h_2, k_2), semi-major axis a_2 and semi-minor axis b_2 is defined. Based on the fact that the definition of both E_1 and E_2 is dependent on the common NOI, their intersection will always result in a set of intersection points (ext I_p) of which one set inadvertently identifies the position of the NOI. However and with reference to Fig. 2, identifying the intersection point that denotes the exact position of the NOI tends to become a cumbersome task when the intersection between E_1 and E_2 results in more than two I_p. Ultimately, the need for a practical way to differentiate intersection coordinates between E_1 and E_2 that define the position of the NOI from those that come about as a direct consequence of the general geometry arises. To this effect, the classical trilateration process which is a feature of most hyperbolic-driven positioning techniques is usually invoked [8]. In general, trilateration is a multilateration process that locates an NOI using exactly three vantage points ($VP_{i=1,2,3}$).

In the scenario depicted by both Figs. 1 and 2, VP_1 would be the reference node pairing between RN_1 and RN_2 that defines E_1, and VP_2 would be the reference node pairing between RN_2 and RN_3 that defines E_2. Introducing a third vantage point just as the trilateration process postulates introduce a third ellipse which brings us a step closer to resolving the 'coordinate of the NOI' ambiguity problem. By introducing another reference node RN_4, and considering the vantage point that would bring about the pairing between itself and any of the previously defined three reference nodes, a third ellipse E_3 with centre coordinate (h_3, k_3), semi-major axis a_3 and semi-minor axis b_3 is defined. As before, by virtue of all three ellipses definition dependence on the NOI, there will be one common coordinate between all three ellipses when they intersect. However, when they do intersect, there will be quite a number of intersection coordinates between the vantage point pairings but there will only be one unique intersection coordinate for the intersection of all three conic sections. That unique coordinate of intersection is (x_{noi}, y_{noi}) and as a consequence, the location of the NOI. At this junction, it is noteworthy to mention that the success of the described trilateration process is partially dependent on the proper placement of the reference nodes in a defined indoor environment prior to its execution [9]. Having mentioned that, a clear guide to the proper placement of reference nodes in a defined environment, as well as the inadvertent limitations that comes with it, is yet to be proposed in any literature. Fig. 3 depicts the aerial view of a typically effective placement configuration of all four reference nodes required for the trilateration process. The reference node pairings RN_1–RN_2, RN_1–RN_3 and RN_1–RN_4 assume the form of VP_1 (E_1), VP_2 (E_2) and VP_3 (E_3), respectively, and the TSOA trilateration process is completed accordingly to determine the coordinates of the NOI [8].

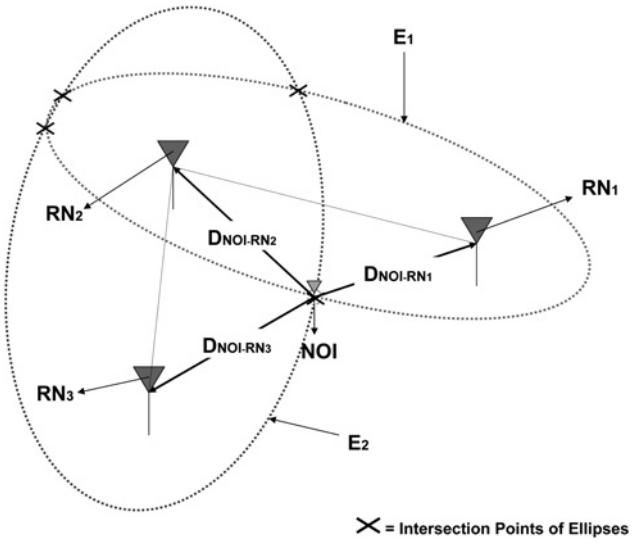

Fig. 2 *Generation of two ellipses using three RNs*

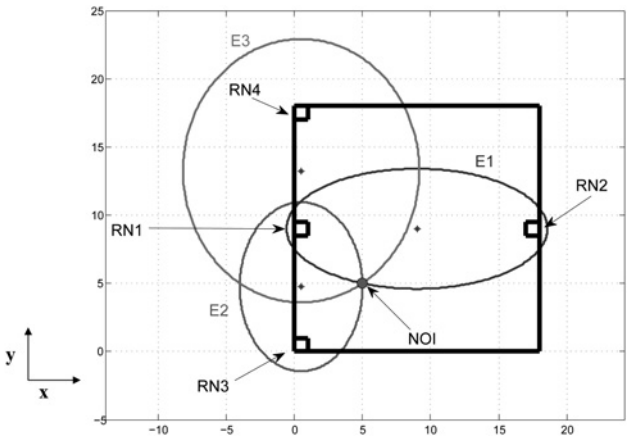

Fig. 3 *Generation of three ellipses using four RNs*

3 Proposed TROA technique

3.1 Optimum two-dimensional (2D) solution space

The 2D solution space of our proposed system is optimised for position estimation in both a square- and a rectangular-shaped indoor environment, and its setup in both quadrilaterals is depicted in Fig. 4. Prior to its setup in the environment, the value of 'A', which would intuitively always be the largest distance in both quadrilaterals, is determined ($A = \sqrt{2\,L^2}$ for the square and $A = \sqrt{L^2 + B^2}$ for the rectangle where L and B are the respective lengths and breadths of the quadrilaterals). This is done to ensure that all signal propagation in both cases is within the indoor UWB transmission range (R_{UWB}) which is typically less than or equal to 30 m [12]. To this effect, we define any square- or rectangular-shaped indoor environment that satisfies the condition of $A \leq R_{\mathrm{UWB}}$ as our 'optimum 2D solution space (O2SS)'. In an event of the TROA system being setup outside the O2SS, there will be regions with no signal propagation, and this would lead to a high reduction in the performance of the system and ultimately a failure of the localisation task.

3.2 TROA multilateration

In contrast to both the conventional TOA- and TSOA-based multilateration techniques that require either an active or a semi-passive NOI to enable signal propagation from it (the NOI) to the relevant reference nodes, TROA is conceived to rely wholly on an inherently passive NOI. In most indoor residential applications, the NOI tends to range from secondary targets such as key electrical appliances and other non-electronic devices to much more primary and inherently animate targets such as the human body. For position estimation using our proposed method, the NOI that could either be a primary or secondary target is equipped with a passive lightweight material of known electrical properties (i.e. conductivity, permittivity, loss tangent, dielectric constant). In [13], we showed that based on the reflection properties of UWB signals as well as having a priori knowledge of the electrical properties of the material that is used to make up an object of interest (lightweight material attached to the NOI in this scenario), it is possible to determine and predict the expected reflected waveform at any UWB receiver (reference node in this scenario) when a UWB signal is incident on the object of interest. Taking this into consideration, TROA multilateration is initially defined in accordance with that which is depicted in Fig. 5. With reference to Fig. 5, TROA replaces TSOA's dependence on RN_1 and RN_2 with a UWB transmitter (T_x) and a UWB receiver (R_{x1}), respectively. When T_x transmits a UWB signal, a version of it will be received at R_{x1} by virtue of the LOS provisioning at a distance of D_{LOS}, and after a time delay which is brought about by the reflection of the UWB signal off the lightweight material attached to the NOI, another version of the signal is also received at R_{x1}.

Considering a simplistic albeit realistic two-path propagation model and a square-shaped indoor environment, once the environment gets tested for

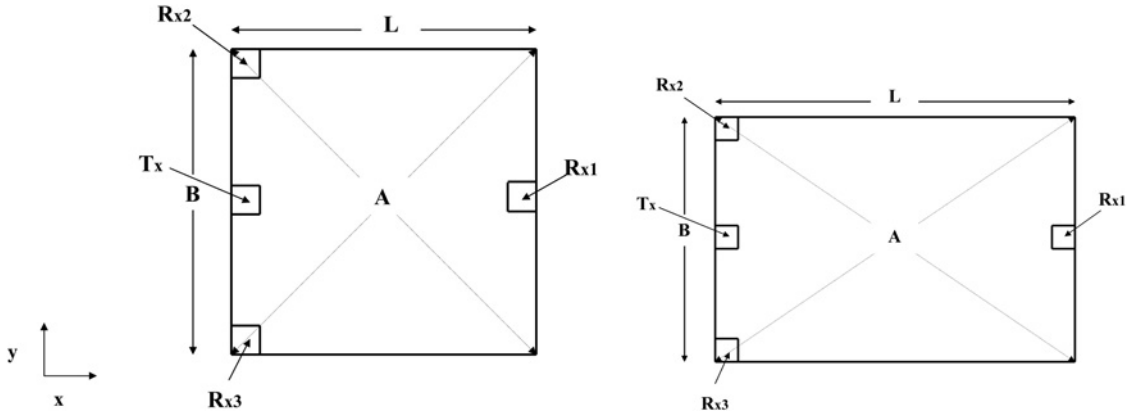

Fig. 4 *Aerial view of TROA system setup for a square- and rectangular-shaped indoor environment*

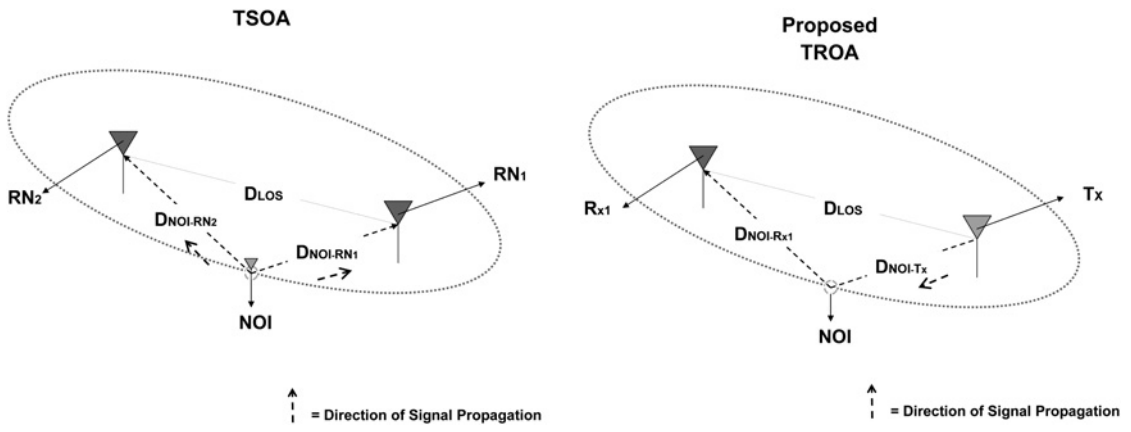

Fig. 5 *Generation of ellipses using TSOA and TROA multilateration approaches*

doi: 10.1049/iet-com.2013.0815

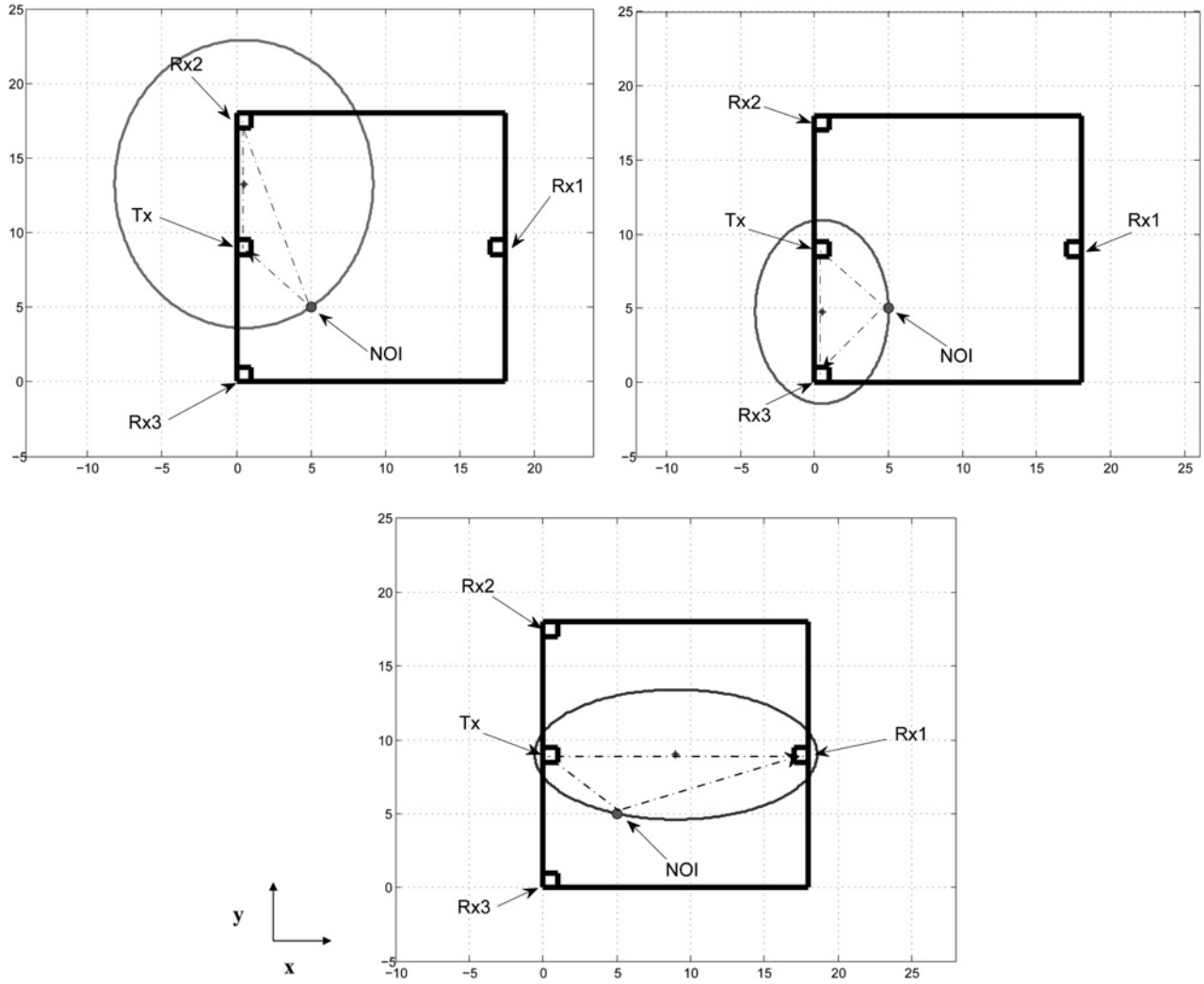

Fig. 6 *Generation of ellipses using proposed TROA approach*

compliance with the O2SS requirement and passes it (i.e. $A \leq R_{\mathrm{UWB}}$), a transmitter (T_x) and three receivers (R_{x1}, R_{x2} and R_{x3}) are deployed in the square as thus. Likening L and B which are defined in Fig. 4 L lies on and spans along the x axis while B lies on and spans along the y axis to the typical x- and y-axis on a 2D x–y grid, respectively, T_x is deployed at coordinate ($0.5p$, $0.5B$), R_{x1} is deployed at coordinate ($0.5p$, $0.5B$), R_{x1} is deployed at coordinate ($L - 0.5p$, $0.5B$), R_{x2} is deployed at coordinate ($0.5p$, $B - 0.5p$) and R_{x3} is deployed at coordinate ($0.5p$, $0.5p$), where p is strictly an arbitrary positive integer that enforces a displacement of both the transmitter or receivers from the edges of the O2SS.

In liaison with Fig. 6, VP_1 becomes the pairing between T_x and R_{x2} whereas VP_2 and VP_3 become the pairings between T_x and R_{x3} and T_x and R_{x1}, respectively. D_{LOS1}, D_{LOS2} and D_{LOS3} are the respective LOS separation distances between the VP_1, VP_2 and VP_3 pairings. Considering VP_1, when an UWB signal $x(t)$ is transmitted by T_x, $x'(t)$ is received by R_{x2} at time t_1 by virtue of the LOS provisioning. At time t_2, $s(t)$ is also received by R_{x2} by virtue of $x(t)$ reflecting off the NOI. Since α is the time delay between the reception of $x'(t)$ and $s(t)$, considering the ideal nature of the assumed environment, α is determined signal processing-wise by means of cross correlating $s(t)$ and $x(t)$ [i.e. $R_{sx}(\tau)$]. A simple plot of $R_{sx}(\tau)$ will lead a single peak occurring at the point where $\tau = \alpha$; and hence the value of α can be easily deduced from the plot. However this can only be done by an initial estimation of $s(t)$ which is achieved by a convolution between $x(t)$, the impulse response of the indoor UWB channel $h(t)$ and the reflection coefficient of the UWB signal $r(t)$ [12]. A multiplication of α with c and then adding it to D_{LOS1} generates the 'range sum' associated with VP_1. Repeating the same process for both VP_2 and VP_3 generates the range sum associated with it too.

3.3 Conic section definition and NOI identification

With reference to the general equation of an ellipse given by (1); and taking all three vantage points into consideration, 'a_i' is defined as half the range sum (i.e. range sum/2) and 'b_i' is defined as $a_i\sqrt{1 - e_i^2}$, where 'e_i' denotes the eccentricity of the ellipse. e_i in turn is defined as f_i/a_i where 'f_i' is half the distance between the two foci of the ellipse. Consequently, 'f_i' can be re-defined as half the distance between the LOS separation between T_x and the corresponding receivers (i.e. $f_1 = \mathrm{D}_{\mathrm{LOS1}}/2$ for VP_1, $f_2 = \mathrm{D}_{\mathrm{LOS2}}/2$ for VP_2 and $f_3 = \mathrm{D}_{\mathrm{LOS3}}/2$ for VP_3). Just as Fig. 6 depicts it, for all three vantage points, three ellipses E_1, E_2 and E_3 which are, respectively, centred at ($0.5p$, $((L - 0.5) + (L/2))/2$), ($0.5p$, $0.5f_2$) and ($0.5f_3$, $0.5L$) are constructed accordingly. Usually, at this stage of the multilateration process, trilateration is invoked to determine the coordinate of the NOI just as we discussed earlier for the TSOA scenario. However, for our proposed TROA, we perform the trilateration process in a

non-conventional manner by a series of elliptical grouping and subsequent comparison. Essentially, the coordinate of the NOI's location is determined by an initial grouping of the defined ellipses; and thereafter a direct comparison of their intersection points for similarities. For a given execution cycle, ellipses E_1 and E_2 are grouped; and their intersection coordinates $\{(x(1), y(1))$ and $(x(2), y(2))\}$ are determined. In a similar manner, ellipses E_1 and E_3 are also grouped and their intersection coordinates $\{(x(3), y(3))$ and $(x(4), y(4))\}$ are also determined. With a combination of four intersection coordinates determined for both groupings, the current execution cycle is concluded by identifying a pair of coordinates in both groups that have similar values. These identified similar values inadvertently denote the coordinate of the NOI, and ultimately its location in the given indoor environment.

4 UWB communication channel consideration

4.1 UWB transmit signal

The UWB transmit signal $x(t)$ depicted in Fig. 7 typically takes the form of the second derivative of the Gaussian impulse function. With ΔT defined as the nominal time duration of $x(t)$, (2) gives its mathematical representation [12, 14]

$$x(t) = \left(1 - 16\pi\left(\frac{t}{\Delta T}\right)^2\right)e^{-8\pi(t/\Delta T)^2} \tag{2}$$

The use of this impulse function derivative as a UWB transmit signal is made possible by carefully allocating ΔT specific values which ensures that the pulse width of the signal is approximately 0.39 ns [12]. This careful allocation results in a −10 dB bandwidth of 7.5 GHz with a maximum spectrum occurring at 5.78 GHz. This coincides with the maximum power spectral density (PSD) allowed by the Federal Communications Commission for UWB communications [12, 15]. With the primary target application for the proposed TROA technique being indoor medical and bio-medical applications, modern literature informs us that theoretically, UWB communications and specifically UWB signals have the potential to enable these applications with an acceptable time delay resolution of 50 cm or better [16]. However, multipath-driven time delays expected in a practical indoor environment typically depend on the propagation scenario (i.e. LOS or NLOS) and type of building (i.e. residential or commercial). In [17], the authors have presented typical time delay values for a varied albeit familiar range of transceiver (i.e. $T_x - R_x$) separation distances.

4.2 UWB channel model

Generally, there are two approaches taken in the modelling of the UWB communication channel namely the widely known and accepted empirical approach [12, 18, 19] and the physics-based approach [18, 19]. In contrast to the physics-based approach and because of the inadvertent complexity in modelling pulse distortions, empirical approaches are not readily available in a generalised closed form, and this is where physics-based modelling becomes relevant [19]. At this junction, it is noteworthy to mention that in physics, signal distortions owing to reflections are fundamentally dissimilar to signal distortions owing to diffraction [19].

From a multilateration vantage point, the parameter of utmost importance is the first arriving multipath component (MPC) of the originally transmitted UWB signal [8, 9]. Nevertheless, the successful detection and subsequent estimation of this MPC at a receiver end is in most cases significantly hindered by the environmentally driven reflections and diffractions. This hindrance brings about a need to model the UWB communication channel in an attempt to cater for the destructive effects (i.e. pulse distortions) reflections and diffractions will have on the transmitted UWB signal. The physics-based approach models the indoor UWB communication channel as a collation of individually localised scattering centre ($\boldsymbol{S}_{i=1,2,3,\ldots,\infty}$) models similar to that which Fig. 8 depicts.

For the distortion model depicted in Fig. 8 which typifies the conventional and well-studied two-ray indoor communications model that is used in a lot of UWB applications, there are three scattering centres ($\boldsymbol{S}_{i=1,2,3}$) and each of them characterises the distortion of the UWB signal in its region by means of the impulse response of the UWB signal to the reflection or diffraction brought about by the surrounding inanimate object(s). The characteristic impulse response that corresponds to each of the scattering centres is

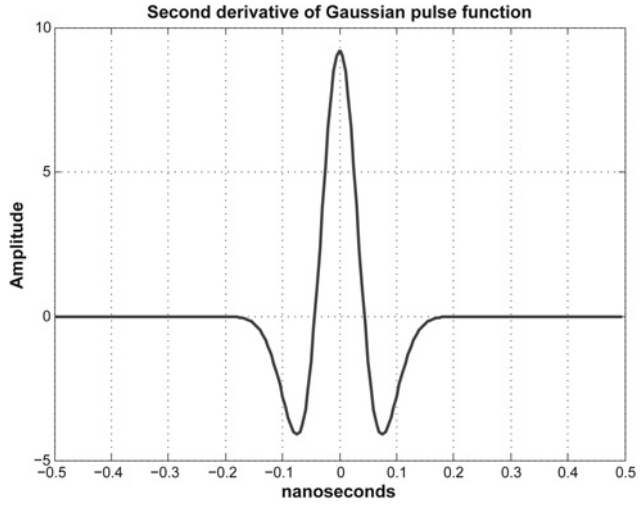

Fig. 7 *UWB signal: second derivative of Gaussian impulse*

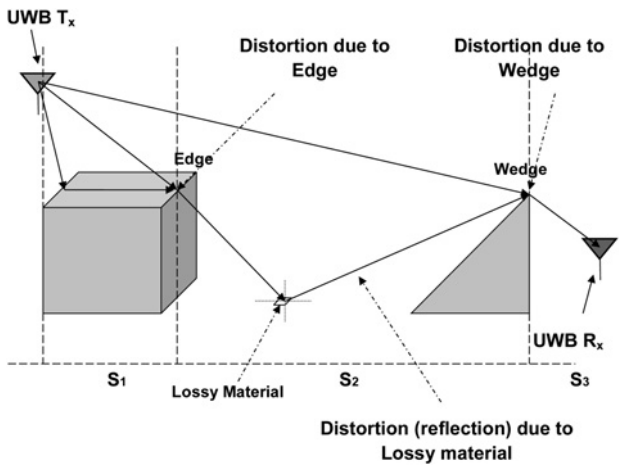

Fig. 8 *Physics-based pulse distortion model*

doi: 10.1049/iet-com.2013.0815

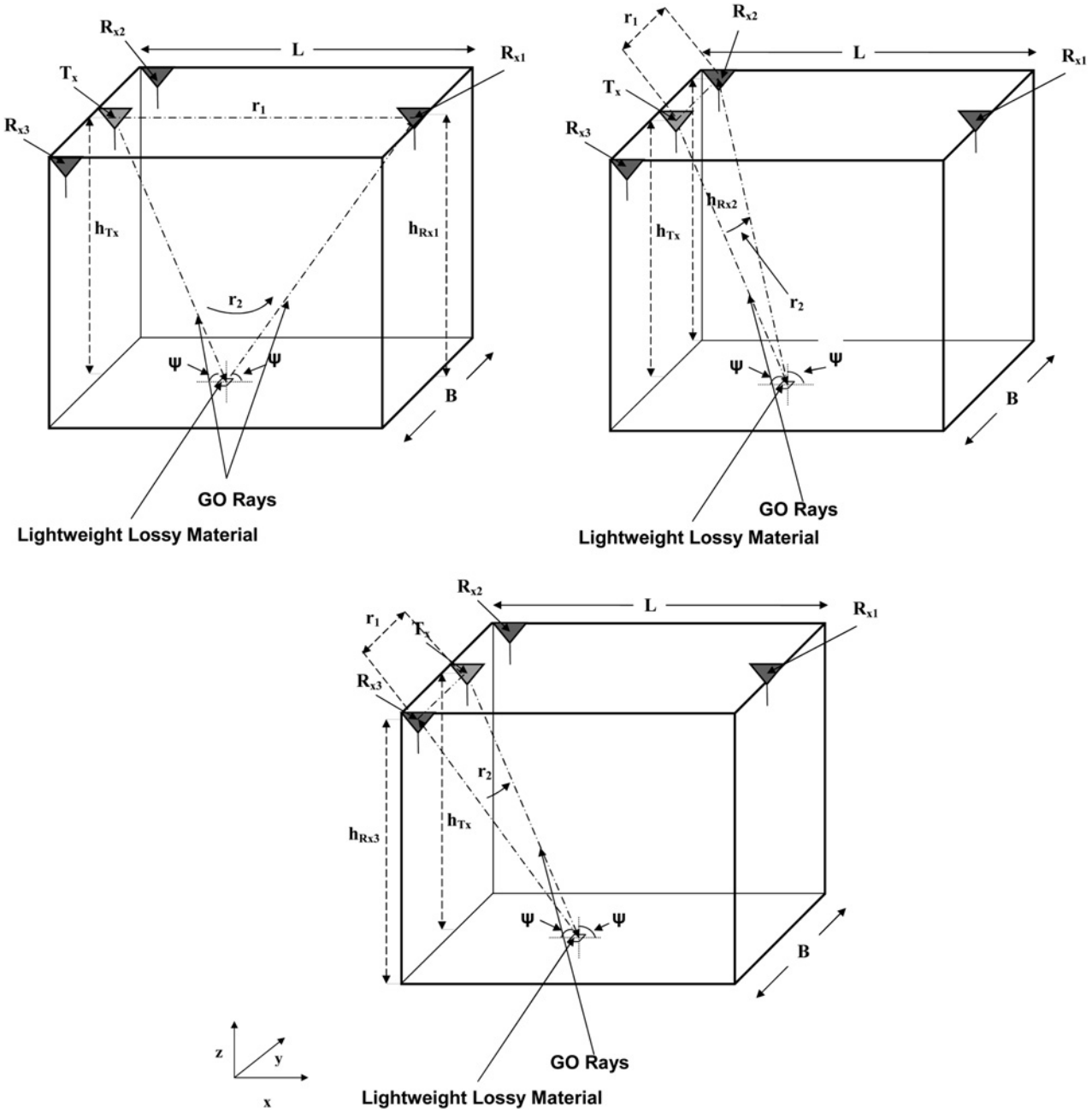

Fig. 9 *UWB channel model description for proposed TROA*

well documented in [18, 19]. Additionally, at any given time, the arrival path of the UWB signal into scattering centre S_i is governed by the departure trajectory of the signal arriving from the preceding scattering centre (i.e. S_{i-1}).

Having mentioned that, for this work we focus wholly on and base the modelling of the UWB communication channel entirely on the physics-based approach that relates to S_2 in Fig. 8 when it is considered as an isolated scattering centre. As shown in Fig. 9, for our channel model, the dependency of the arrival path of the UWB signal on the departure trajectory of the signal from the preceding scattering centre is replaced by a fixed omni-directional UWB transmitter (T_x). Just as Fig. 9 depicts it, T_x and the respective receivers are placed at the corners of the ceiling of a defined O2SS at the coordinates which we defined in verbatim in the previous section. With reference to [19] and considering the vantage point that pairs T_x with R_{x1} (i.e. VP_3 from the previous section), for non-zero values of the incidence angle ψ of the transmitted UWB signal $x(t)$ where ε_r and σ refer to the relative dielectric constant of the lossy material and its conductivity, respectively, the transfer function and its analogous impulse response $h(\tau)$ associated with $x(t)$ when it suffers some distortion pulsewise in a scattering centre similar to S_2 is as a direct consequence of geometric optics rays (i.e. reflection off the lossy material) and is defined as

$$h(\tau) = \frac{1}{r_1}\delta(\tau) + \frac{1}{r_2}R_1(\tau) \otimes \delta(\tau - \tau_1) \tag{3}$$

where $R_1(t) = \pm K\delta(t) + R_{01}(t)$, $R_{01}(t)$ which in turn is defined

as the reflection coefficient of the transmitted UWB signal is denoted by

$$R_{01}(t) = \left(\frac{4\,k}{1-k^2}\right)\left(\frac{e^{-at}}{t}\right)\sum_{n=1}^{\infty}(-1)^{n+1}nK^nI_n(at)$$

$$\tau_1 = \frac{(r_2-r_1)}{c}, \quad K = \frac{(1-k)}{(1+k)}$$

$$k = \begin{cases} \sqrt{\epsilon_r - \cos^2\psi}/(\epsilon_r \sin\psi) & \text{for vertical polarisation} \\ \sin\psi/\sqrt{\epsilon_r - \cos^2\psi} & \text{for horizontal polarisation} \end{cases}$$

$$\psi = \arctan\frac{(h_{T_x}+h_{R_x})}{d}, \quad r_1 = \sqrt{(h_{T_x}-h_{R_x})^2+d^2}$$

$$r_2 = \sqrt{\left(h_{T_x}+h_{R_x}\right)^2+d^2}, \quad a = \frac{120\pi\sigma c}{2\epsilon_r}$$

Just as Qiu [18, 19] has pointed out extensively, based on the fact that $I_n(at)$ is the modified Bessel function, for values of $at \leq 1$, $R_{01}(t)$ can be manipulated and finally reduced to

$$R_{01}(t) \simeq K\frac{2\,k}{1-k^2}e^{-(1+K)at}$$

Without loss of generality, in our indoor environment and with reference to Fig. 9, the values of h_{T_x}, $h_{R_{x1}}$, $h_{R_{x2}}$ and $h_{R_{x3}}$ are the same; and hence ψ, r_1 and r_2 can all be, respectively, re-defined as

$$\psi = \arctan\frac{2\,h}{d}, \quad r_1 = d, \quad r_2 = \sqrt{2\,h^2+d^2}$$

where

$$h = h_{T_x} = h_{R_{x1}} = h_{R_{x2}} = h_{R_{x3}}$$

It suffices to say that the impulse response definition for the vantage point that pairs T_x with R_{x1} also follows through from the other two vantage points that pair T_x with R_{x3} and R_{x2}, respectively, just as Fig. 9 illustrates. Intuitively, the values for the UWB channel model parameters wholly depend on the lossy material being used for the localisation task. However typical values of ε_r and σ are 2.07 and 0.005, respectively, when the lossy material being considered is the material used to make a wooden door frame [20]. When the lossy material being considered is the material used to make a cement surface, the values of ε_r and σ are 6 and 0.0166, respectively [12]. The primary aim of explicitly defining the UWB channel model is to demonstrate the theoretical feasibility of our approach in potential real-world experiments. The indirect implications of the simplified UWB channel model on the validation of our technique were considered. As we demonstrate in Section 5, these implications are in the form of the defined standard deviation range of the normally distributed TOA measurement variation.

4.3 UWB channel model for multiple UWB signal interactions

Fig. 10 depicts the structure of a typical UWB channel model for multiple signal $x(t)$ interactions when the vantage point that pairs T_x with R_{x1} is considered. As with the previous modelling process, the modelling of the UWB multipath

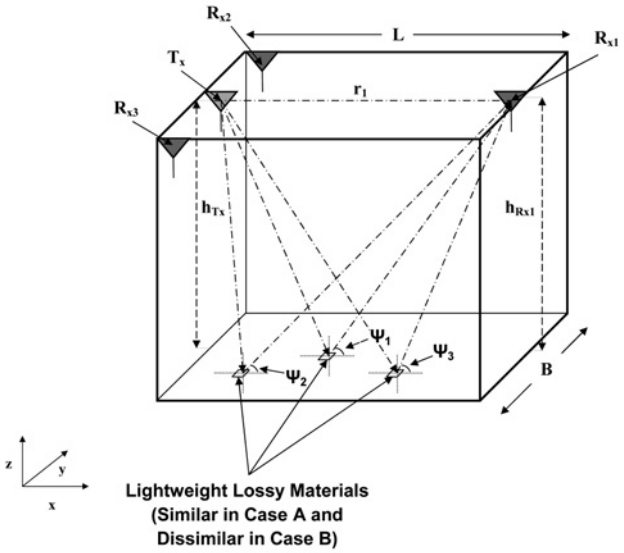

Fig. 10 *UWB multipath channel model description*

channel is based on the physics-based approach that corresponds to the isolated scattering centre S_2 in Fig. 8. Depending on the specified indoor UWB application, multiple interactions between the transmitted UWB signal $x(t)$ and surrounding lossy materials which are either similar or dissimilar to the NOI, occurs [18, 19]. Hence it is sufficient to model the impulse response of the channel to both cases (i.e. cases A and B) independently. Case 'A' refers to a scenario whereby the surrounding lossy materials in the defined O2SS are similar to the NOI in terms of their ϵ_r and σ parameter values; and case 'B' refers to a scenario whereby the surrounding lossy materials in the defined O2SS have dissimilar parameter values to the NOI. The impulse responses $h_1(\tau)$ and $h_2(\tau)$ of the multipath channel for both cases A and B can be derived, respectively, from the generalised multipath definition explicitly detailed in [18, 19].

4.4 UWB multipath channel power delay profile

For a given impulse response $h(t)$ of a multipath channel, a measure of how dispersed the received signal is with respect to the originally transmitted UWB signal $x(t)$, is called the 'power delay profile' [21, 22]. Essentially, the power delay profile indicates the degree of dispersion of the

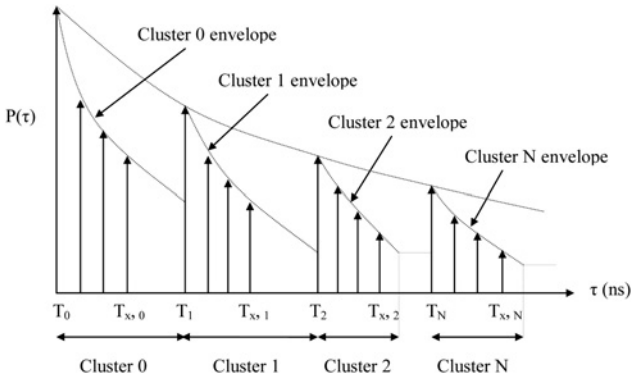

Fig. 11 *Illustration of power delay profile of the UWB multipath channel*

doi: 10.1049/iet-com.2013.0815

received signal and is measured as the spatial average of $|h(t)|^2$ [21, 22]. With the physics-based modelling process of $h(t)$ being partially dependent on the electrical properties of the lossy material and the NOI inadvertently, the TOA of the MPCs also becomes dependent on the electrical properties of the lossy material. Hence the power delay profile for every defined propagation scenario is dissimilar. However, just as Fig. 11 depicts it, the power delay profile for UWB channels typically assumes an exponential shape within each cluster and the mean energy of each cluster assumes an exponentially decaying outlook [21, 22]. T_i refers to the first MPC in cluster i whereas $T_{x,i}$ refers to the xth MPC in cluster i. Numerical values for path arrival times and cluster power corresponding to the LOS and NLOS in residential, office, industrial and outdoor environment have been reported in [23].

5 Validation of technique

5.1 TROA against TOA against TSOA (effectiveness test)

Innately, the effectiveness of any geometric multilateration technique relies heavily on the accuracy of the initially obtained TOA measurements. It suffices to hypothesise that a necessary comparison between two or more multilateration techniques in an attempt to determine their order of effectiveness becomes one that has to be driven by an introduced and calculated variation in the TOA measurements. To this effect; and considering LOS propagation conditions (i.e. propagation path is not obstructed by a physical object either fully or partially), we modelled this TOA measurement variation for all three methods (i.e. TROA, TOA and TSOA) as a normally distributed Gaussian random variable $N(0, \sigma^2_{\text{TOA}})$, and generated 1000 random samples each for a fixed range of standard deviation (σ_{TOA}) of the TOA measurements. This range of σ_{TOA} was fixed to coincide with a localisation accuracy that spans from 3 to 30 cm (i.e. 0.1 to 1 ns). We subjected the NOI to a number of fixed coordinates and for demonstration purposes in this paper, we focus on and present the results for three randomly picked coordinates namely (5,5), (9,14) and (12,4).

The initial TOA measurements that result in the determination of all three defined coordinates using TROA, TOA and TSOA are, respectively, corrupted with the randomly generated Gaussian noise samples over the defined σ_{TOA} range; and the NOI's location is subsequently redetermined.

Figs. 12–14 show the resultant σ_{TOA} against MSE plots for the specified σ_{TOA} range when the fixed coordinates are compared with the coordinates redetermined using the corrupted TOA measurements. These plots clearly show that a corruption in the TOA measurements just as it is bound to happen in practice by means of interference, pulse distortion or unresolved multipath signals, has as expected a negative effect on the localisation effectiveness on all three methods. In an apparent disagreement with literature, these plots also show that TSOA has a better performance than TOA. However, this better performance is attributed to the extra receiver requirement TSOA needs to do the same positioning task as TOA (i.e. TSOA = $4R_x$ and TOA = $3R_x$); and hence backing up literatures statement that TSOA does not necessarily provide any additional performance advantages over existing multilateration techniques. Finally and most significantly, it is also clear to see that TROA will always have a better location estimation effectiveness in terms of MSE when compared to the other two methods over the defined σ_{TOA} range.

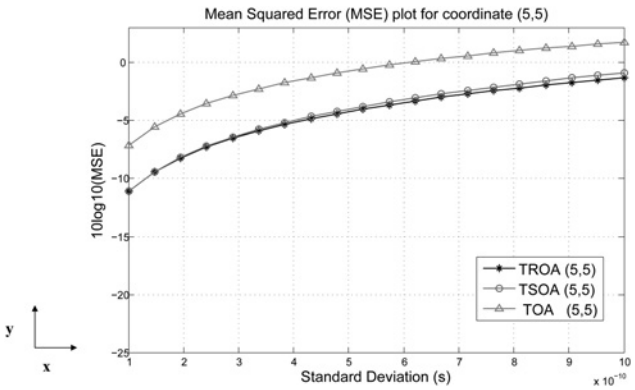

Fig. 12 *MSE comparison for coordinate (5,5)*

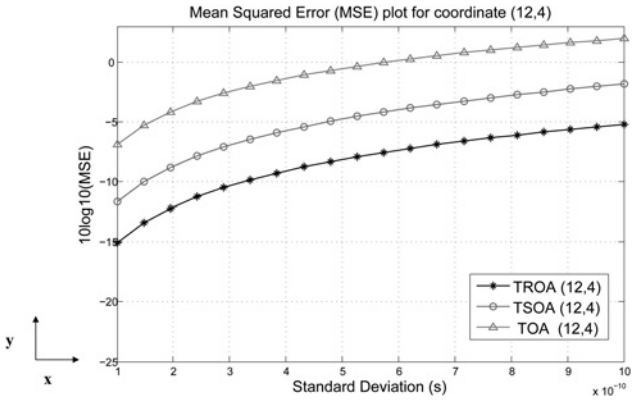

Fig. 13 *MSE comparison for coordinate (12,4)*

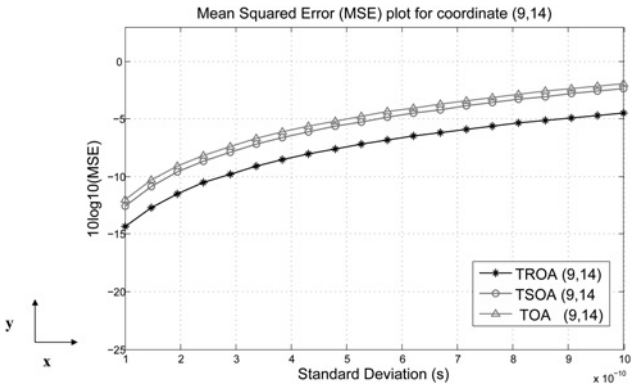

Fig. 14 *MSE comparison for coordinate (9,14)*

5.2 Efficiency test of TROA via CRLB

To study the efficiency of the proposed TROA approach, we compare the MSEs of the parameter estimation to their corresponding CRLBs. The CRLBs provide a lower bound on the covariance that is asymptotically achievable by any unbiased estimation algorithm based on the measurement vector $\boldsymbol{z}$ [24]. It is calculated from the inverse of the Fisher information matrix (FIM) $\boldsymbol{J}$. Let the target location $x \in \mathbb{R}^2$ be the parameter of interest and $\hat{x}$ an estimate of it obtained

from the measurement vector $\boldsymbol{z}$. Then the error covariance $\mathbb{E}[(\hat{x}-x)(\hat{x}-x)^{\mathrm{T}}]$ is bounded below by

$$\mathbb{E}[(\hat{x}-x)(\hat{x}-x)^{\mathrm{T}}] \geq \boldsymbol{J}^{-1} \tag{4}$$

$$\boldsymbol{J} = \mathbb{E}\left[\nabla_x \ln\, p(\boldsymbol{z}|x)(\nabla_x \ln\, p(\boldsymbol{z}|x))^{\mathrm{T}}\right] \tag{5}$$

where $\mathbb{E}[.]$ determines the expectation value.

Additionally, the unknown time of emission t_0 is to be estimated. Therefore for localisation, the parameter of interest is the extended position state of the emitter

$$x^{(+)} = \left(t_0, x^{\mathrm{T}}\right)^{\mathrm{T}} \in \mathbb{R}^3 \tag{6}$$

Given the measurement vector $\boldsymbol{z}_t$, the CRLB for TROA localisation for one time step is computed from the inverse of the Fisher information for TROA, a 3×3 matrix

$$\boldsymbol{J}_t = \frac{\partial \boldsymbol{h}_t^{\mathrm{T}}}{\partial x^{(+)}} \boldsymbol{R}_t^{-1} \frac{\partial \boldsymbol{h}_t}{\partial x^{(+)}} \tag{7}$$

The Jacobian of the measurement function is

$$\frac{\partial \boldsymbol{h}_t}{\partial x^{(+)}} = \begin{pmatrix} \frac{\partial h_1}{\partial t_0} & \frac{\partial h_1}{\partial x} & \frac{\partial h_1}{\partial y} \\ \frac{\partial h_2}{\partial t_0} & \frac{\partial h_2}{\partial x} & \frac{lh_2}{\partial y} \\ \frac{\partial h_3}{\partial t_0} & \frac{\partial h_3}{\partial x} & \frac{\partial h_3}{\partial y} \end{pmatrix} = \begin{pmatrix} c & \frac{x-x_1}{r_1} & \frac{y-y_1}{r_1} \\ c & \frac{x-x_2}{r_2} & \frac{y-y_2}{r_2} \\ c & \frac{x-x_3}{r_3} & \frac{y-y_3}{r_3} \end{pmatrix} \tag{8}$$

The computation of the FIM follows as

$$\begin{aligned} \boldsymbol{J}_t &= \begin{pmatrix} c & c & c \\ \frac{x-x_1}{r_1} & \frac{x-x_2}{r_2} & \frac{x-x_3}{r_3} \\ \frac{y-y_1}{r_1} & \frac{y-y_2}{r_2} & \frac{y-y_3}{r_3} \end{pmatrix} \times \begin{pmatrix} \frac{1}{\sigma_1^2} & 0 & 0 \\ 0 & \frac{1}{\sigma_2^2} & 0 \\ 0 & 0 & \frac{1}{\sigma_3^2} \end{pmatrix} \\ &\quad \times \begin{pmatrix} c & \frac{x-x_1}{r_1} & \frac{y-y_1}{r_1} \\ c & \frac{x-x_2}{r_2} & \frac{y-y_2}{r_2} \\ c & \frac{x-x_3}{r_3} & \frac{y-y_3}{r_3} \end{pmatrix} \\ &= \sum_{i=1}^{3} \begin{pmatrix} \frac{c^2}{\sigma_i^2} & \frac{c}{\sigma_i^2}\frac{x-x_i}{r_i} & \frac{c}{\sigma_i^2}\frac{y-y_i}{r_i} \\ \frac{c}{\sigma_i^2}\frac{x-x_i}{r_i} & \frac{1}{\sigma_i^2}\frac{(x-x_i)^2}{r_i^2} & \frac{1}{\sigma_i^2}\frac{(x-x_i)(y-y_i)}{r_i^2} \\ \frac{c}{\sigma_i^2}\frac{y-y_i}{r_i} & \frac{1}{\sigma_i^2}\frac{(x-x_i)(y-y_i)}{r_i^2} & \frac{1}{\sigma_i^2}\frac{(y-y_i)^2}{r_i^2} \end{pmatrix} \end{aligned} \tag{9}$$

The Fisher information can be expressed by

$$\boldsymbol{J}_t = \begin{pmatrix} J_{11} & J_{12} & J_{13} \\ J_{21} & J_{22} & J_{23} \\ J_{31} & J_{32} & J_{33} \end{pmatrix} = \begin{pmatrix} J_t & J_{t,\mathrm{pos}} \\ J_{\mathrm{pos},t} & \boldsymbol{J}_{\mathrm{pos}} \end{pmatrix} \tag{10}$$

where $\boldsymbol{J}_{\mathrm{pos}}$ is the Fisher information of the position space, J_t.

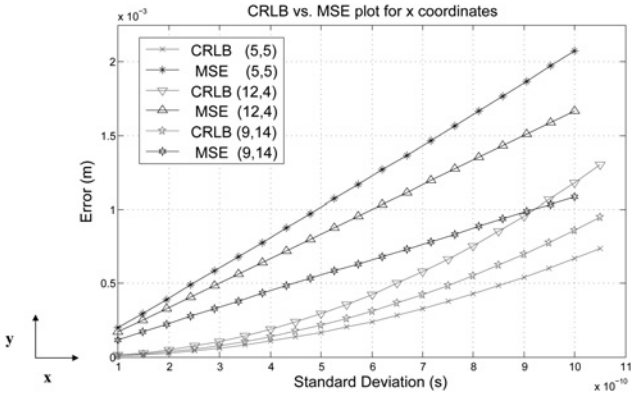

Fig. 15 *CRLB against MSE comparison for x coordinates of (5,5), (12,4) and (9,14)*

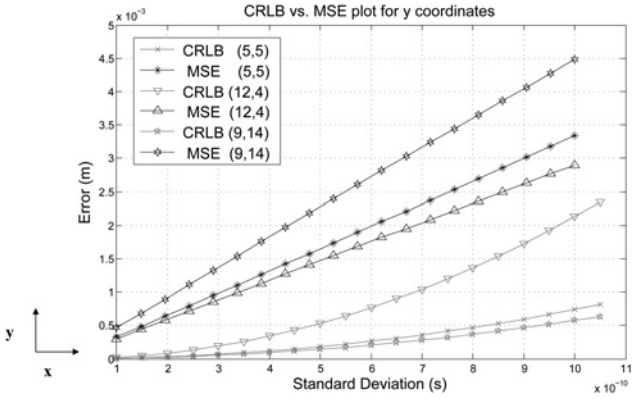

Fig. 16 *CRLB against MSE comparison for y coordinates of (5,5), (12,4) and (9,14)*

The FIM of the time space and the others are the cross terms. The CRLB of the position space can be computed using the matrix inversion lemma [24]. The time of emission is treated as nuisance parameter. It can be shown that $\boldsymbol{J}_{\mathrm{pos}} = \boldsymbol{J}_{\Delta ti}$, $i = 1, \ldots, 3$.

Figs. 15 and 16 illustrate the estimation performance of our approach for the x coordinate and y coordinate of the NOI, respectively. The localisation performance was studied for three different positions of the NOI within the indoor environment of interest. We considered the following positions: $(x, y) = (5, 5)$, $(12, 4)$, $(9, 14)$. In these three cases, the TROA approach shows good performances where the MSEs are close to their respective CRLBs.

6 Conclusion

This paper presented a novel UWB-driven multilateration technique for position estimation in an indoor environment. The presented approach exploits the inherent properties of UWB signal propagation and its definition is in conjunction with the operational principles of the lesser studied TSOA position estimation technique. In this work we have studied the accuracy of the proposed approach for a network of three receivers and one transmitter. By means of a series of statistically driven MSE analyses, we have shown that in comparison with TOA and TSOA, the proposed TROA technique possesses a much higher accuracy with regards to position estimation. The CRLBs were also computed using TROA measurement set; and we have been able to show

doi: 10.1049/iet-com.2013.0815

that the proposed TROA technique shows good performances when the CRLB is directly compared with the MSE. We have studied the influence of the position of the NOI within the indoor environment and relatively to the network of sensors. This latter study could be made more generic by varying the position of the NOI in a continuous fashion within the environment of interest which will provide a means of assessing optimum performances of our system.

7 Acknowledgments

The authors would like to thank the Engineering and Physical Science Council (EPSRC) and DANCER project team at London South Bank University for their financial contribution towards this work.

8 References

1 Yamada, I., Ohtsuki, T., Hisanaga, T., Zheng, L.: 'An indoor position estimation method by maximum likelihood algorithm using RSS'. Proc. SICE Annual Conf., September 2007, pp. 2927–2930
2 Uchitomi, N., Inada, A., Fujimoto, M., Wada, T., Mutsuura, K., Okada, H.: 'Accurate indoor position estimation by swift-communication range recognition (S-CRR) method in passive RFID systems'. Proc. Int. Conf. Indoor Positioning and Indoor Navigation, September 2010, pp. 1–7
3 Hauschildt, D., Kirchhof, N.: 'Improving indoor position estimation by combining active TDOA ultrasound and passive thermal infrared localization'. Proc. IEEE WPNC, April 2011, pp. 94–99
4 Hongliang, R., Meng, M.Q.-H., Lisheng, X.: 'Indoor patient position estimation using particle filtering and wireless body area networks'. Proc. Int. Conf. Engineering in Medicine and Biology Society, August 2007, pp. 2277–2280.
5 Aso, M., Kawabata, M., Hattori, T.: 'A new location estimation method based on maximum likelihood function in cellular systems'. Proc. IEEE Conf. Vehicle Technology, 2001, pp. 106–110
6 Man-Kin Chu, K., Kee-Yin Ng, J., Leung, K.R.P.H.: 'A new approach for locating mobile stations under the statistical directional propagation model'. Proc. Int. Conf. Advanced Information Networking and Applications, April 2006, pp. 932–940
7 Roos, T., Myllymaki, P., Tirri, H.: 'A statistical modeling approach to location estimation', *IEEE Trans. Mob. Comput.*, 2002, **1**, (1), pp. 59–69
8 Munoz, D., Bouchereau, F., Vargas, C., Enriquez-Caldera, R.: 'Position location techniques and applications' (Academic Press, Elsevier, 2009)
9 Liu, Y., Yang, Z.: 'Location, localization, and localizability: location-awareness technology for wireless networks' (Springer, 2011)
10 Kuen-Tsiar, L., Wei-Kai, C.: 'Mobile positioning based on TOA/TSOA/TDOA measurements with NLOS error reduction'. Proc. Int. Symp. Intelligent Signal Processing and Communication Systems, December 2005, pp. 545–548
11 Eisenhart, L.P.: 'Coordinate geometry (reprint)' (Dover, 2005)
12 Ghavami, M., Michael, L.B., Kohno, R.: 'Ultra wideband signals and systems in communication engineering' (Wiley, 2004)
13 Onalaja, O., Ghavami, M.: 'UWB based pre-localisation algorithm for aiding target location in a multipath environment'. Proc. IEEE Int. Conf. Ultra-Wideband, September 2011, pp. 140–144
14 Onalaja, O., Ghavami, M., Adjrad, M.: 'UWB-based elliptical target localization in an indoor environment'. Proc. Int. Workshop on Systems, Signal Processing and their Applications, May 2013, pp. 103–107
15 Popa, A.: 'An optimization of Gaussian UWB pulses'. Proc. Int. Conf. Development and Application Systems, May 2010
16 D'Amico, S., Matteis, M., Rousseaux, O., Philips, K., Gyselinck, B., Neirynck, D., Baschirotto, A.: 'Ultra wide band in medical applications'. Advances in biomedical sensing, measurements, instrumentation and systems (*Lecture Notes in Electrical Engineering* **55**) (Springer, Berlin, Heidelberg, 2010), pp. 43–60
17 Ghassemzadeh, S.S., Greenstein, L.J., Sveinsson, T., Kavcic, A., Tarokh, V.: 'UWB delay profile models for residential and commercial indoor environments', *IEEE Trans. Veh. Technol.*, 2005, **54**, (4), pp. 1235–1244
18 Qiu, R.C.: 'A generalized time domain multipath channel and its application in ultra-wide-band (UWB) wireless optimal receiver design: system performance analysis'. Proc. IEEE Wireless Communications and Networking Conf., March 2004, vol. 2, pp. 901–907
19 Qiu, R.C.: 'A generalized time domain multipath channel and its application in ultra-wideband (UWB) wireless optimal receiver design – part II: physics-based system analysis', *IEEE Trans. Wirel. Commun.*, 2004, **3**, (6), pp. 2312–2324
20 Zhang, N.T., Meng, J.: 'Reflection characteristics analysis of IR-UWB signal'. Proc. Int. Conf. Wireless Communications, Networking and Mobile Computing, October 2008, pp. 1–4
21 Sahinoglu, Z., Gezici, S., Guvenc, I.: 'Ultra-wideband positioning systems: theoretical limits, ranging algorithms, and protocols' (Cambridge University Press, 2008)
22 Llano, G., Cuellar, J.C., Navarro, A.: 'Frequency UWB channel', in Matin, M. (Ed.): 'Ultra wideband communications: novel trends – antennas and propagation', (InTech, 2011), pp. 67–74
23 Jadhavar, B.R., Sontakke, T.R.: 'Simulation and analysis of UWB indoor channel through S–V model for user location detection', *Int. J. Comput. Electr. Eng.*, 2011, **3**, (5), pp. 729–738
24 Kay, S.M.: 'Fundamentals of statistical signal processing: estimation theory' (*Signal Processing Series*) (Prentice-Hall, 1993)